Detailed Real-Time Transient Model of the "Sen" Transformer

Babak Asghari, *Student Member, IEEE*, M. Omar Faruque, *Student Member, IEEE*, and Venkata Dinavahi, *Member, IEEE*

***Abstract*—This paper presents the real-time simulation and control of the "Sen" Transformer (ST) for transmission power-flow regulation. A detailed electromagnetic transient model was developed for the ST embedded in the network, and a comprehensive control technique was proposed for the operation of the ST. To implement the models in real time, a state-of-the-art high performance PC-cluster-based real-time simulator was used. The ST model and the controller are implemented using a custom C program in MATLAB/SIMULINK environment. The execution time of the entire system is only 75 μs on a simulation time-step of 100 μs. Real-time oscilloscope results are provided to show the validity of the model under steady-state and transient conditions.**

***Index Terms*—Electromagnetic transient analysis, power system modeling, real-time systems, "Sen" transformer.**

I. Introduction

THE "Sen" transformer (ST), is a power-flow controller made out of a three-phase transformer with multiple windings in the secondary (known as the compensating windings), each of which has on-load tap-changing capability. In a transmission network with the ST, the compensating windings that are connected in series with the line insert a series voltage whose magnitude and phase angle depend on the tap setting of each winding. The magnitude and phase angle of the required series voltage is determined by the system requirement. However, any series voltage injection in the line can be approximated through the combined contribution from one or two compensating secondary winding(s). The concept of ST, proposed in [1], establishes that in a power system where slow dynamic response is sufficient, the ST can replace the power-electronics-based unified power-flow controller (UPFC). This is further corroborated in [2], where off-line simulation results for both the ST and the UPFC have been compared while using the same transmission network. Further in [3] a novel tap-changing algorithm was proposed to select the contributions from the individual compensating windings in response to a series voltage injection demand. However, in all of these studies a simplified model of the ST was used.

As the ST is a special type of transformer, its model is not readily available in transient simulation programs such as EMTP or PSCAD/EMTDC. Therefore, in [2], [3] ideal single-phase transformer models are employed to construct the ST. Such modeling ignores the mutual coupling between compensating windings, and the nonlinear magnetic characteristic of the ST, thereby producing results which are not a true reflection of its behavior under transient conditions. An accurate and precise model is the foundation of any simulation study, and therefore, a detailed model of the ST is necessary to understand its true response under various operating conditions.

In this paper, a detailed real-time electromagnetic transient model of the ST as a three-phase multi-legged transformer containing three primary and nine secondary windings is described. The linear part of the developed ST model is based on the BCTRAN [4] model, and the non-linear part is based on a piece-wise linear approximation of the B-H curve. The entire ST model and the transmission network is programmed as a C S-function in the MATLAB/SIMULINK environment. The control algorithm for the tap-selection of the ST was also implemented through a C program which determines the tap positions of the compensating windings. An improvement over [3] is achieved by making the control program versatile for the use of either voltage regulation or phase angle regulation or power-flow control with corresponding reference inputs. Detailed tap-changing mechanism described in [3] was implemented through multiple steps for studying the transient response. Both the system and controller models are executed in real-time on an advanced PC-cluster. Real-time oscilloscope results are shown for model validation.

The paper is organized as follows. Section II describes the operation of the ST and the control algorithm for tap selection. Detailed modeling of the ST, electrical network and the controller for transient simulation are described in Section III. Real-time implementation of the entire model on the PC-Cluster is described in Section IV. Section V presents results of the ST simulation for both the steady-state and transient conditions, followed by conclusion in Section VI.

II. ST and Its Control Strategy

The schematic of the ST within a transmission line is shown in Fig. 1. The ST injects a combined compensating voltage, $\mathbf{V_{s's}}$, which is generated from the transformer's secondary windings that are connected in series. The compensating voltage of variable magnitude and variable angle modifies the magnitude and the angle of the sending-end voltage, $\mathbf{V_s}$, to be the effective sending-end voltage, $\mathbf{V_{s'}}$, and therefore, controls the active and reactive power flow in the transmission line independently.

Manuscript received February 6, 2007; revised July 10, 2007. This work was supported by the Natural Sciences and Engineering Research Council of Canada (NSERC). Paper no. TPWRD-00060-2007.

The authors are with the Department of Electrical and Computer Engineering, University of Alberta, Edmonton, AB T6G 2V4 Canada (e-mail: dinavahi@ece.ualberta.ca).

Color versions of one or more of the figures in this paper are available online at http://ieeexplore.ieee.org.

Digital Object Identifier 10.1109/TPWRD.2008.916745

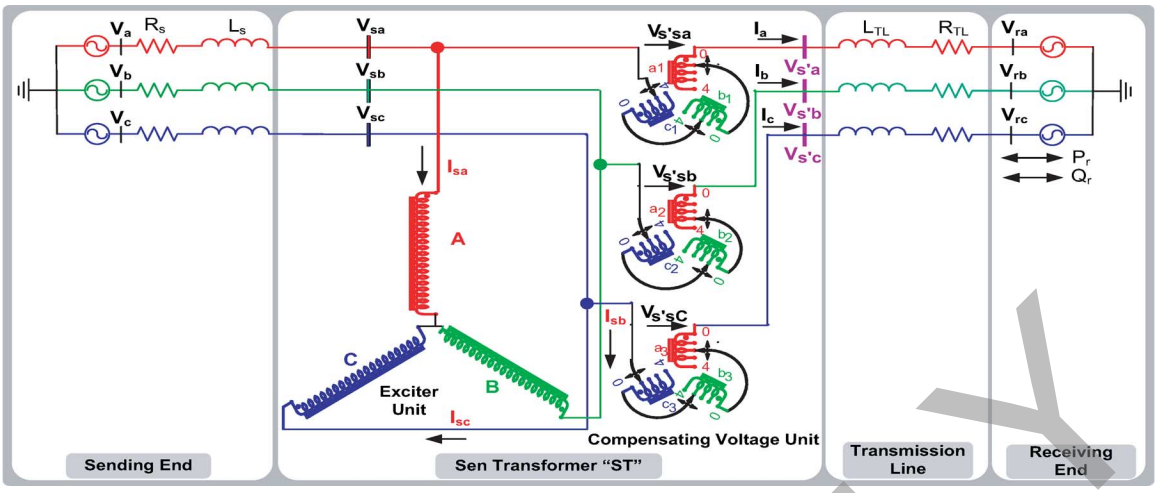

Fig. 1. Schematic of the electrical network and the ST.

A. Operation of the ST and Tap Changing Mechanism

As shown in Fig. 1, the ST has two main units: exciter unit and compensating-voltage unit. The exciter unit consists of Y-connected shunt primary windings (A, B, and C) and the compensating-voltage unit consists of nine secondary windings, three of which are placed on each limb of the core e.g., a_1, a_2, and a_3 on the first limb, b_1, b_2, and b_3 on the second limb, and c_1, c_2, and c_3 on the third limb. The three-phase transmission line voltages ($\mathbf{V_{sa}}$, $\mathbf{V_{sb}}$, and $\mathbf{V_{sc}}$) at the sending-end are applied in shunt to the exciter unit. The induced voltages from three windings that are placed on three different limbs are added through series connection to produce the compensating voltage for injection in series with the transmission line, e.g., a_1, b_1, and c_1 for injection in A-phase, a_2, b_2, and c_2 for injection in B-phase, and a_3, b_3, and c_3 for injection in C-phase. The magnitudes of the components of the three 120° phase-shifted induced voltages are varied through active turns in the compensating windings, and therefore, the composite voltage, $\mathbf{V_{s'_s}}$ becomes variable in magnitude and also in phase angle (0° to 360°).

To perform on-load tap changing operation, generally, a resistor or inductor is used in parallel with the tap-positions to limit the current through a shorting winding segment between two consecutive taps. A detailed description of the tap changing mechanism is described in [3]. Practical transformers with on-load tap changers (OLTC) such as the ones from Reinhausen [5] use taps in the range of 2% to 6.7%. However, in this paper a 5% tap will be used for the ST simulation. The time chosen to move the tap selector between adjacent tap positions is 2 s.

B. Control Algorithm for the ST

By varying the magnitude of $\mathbf{V_{s'_s}}$, and phase angle, β of the injected compensating voltage, the ST can function as 1) voltage regulator, 2) phase angle regulator, or 3) independent power-flow regulator [1]. Due to the discrete nature of the taps of the compensating windings, in most cases, it is not possible to inject the exact amount of required series voltage for a given active and reactive power flow in the line. Any value of $\mathbf{V_{s'_s}}$ can, however, be approximated using several tap combinations of the ST windings, and therefore, a suitable tap selection algorithm is needed to identify the required tap positions, which yields a minimum error.

1) ST Control for Voltage Regulation: As shown in the phasor diagram in Fig. 2(a), the ST as a voltage regulator adds voltage in series and hence changes the phase voltage $\mathbf{V_s}$ to $\mathbf{V_{s'}}$. The added voltage could be either in-phase with $\mathbf{V_s}$ ($\beta = 0°$) or out-of-phase ($\beta = 180°$).

2) ST Control for Phase Angle Regulation: If the ST is used as a phase angle regulator, voltages are added to the line in quadrature with $\mathbf{V_s}$ ($\beta = \pm 90°$), as shown in the phasor diagram in Fig. 2(b).

3) ST Control for Independent Power Flow Regulation: In the ST, both the active and the reactive power flow are independently regulated by changing $\mathbf{V_s}$ to $\mathbf{V'_s}$ through an injection of series voltage, $\mathbf{V_{s'_s}}$, at an angle β with respect to the sending end voltage, $\mathbf{V_s}$. The phasor diagram in Fig. 2(c) illustrates that for this control, it is necessary to produce $\mathbf{V_{s'_s}}$ at any angle β, in the range of 0° to 360°. The required power levels (P_{ref} and Q_{ref}) are the reference inputs in Fig. 2(d) from which $|\mathbf{V_{s'_s}}|$ and β are calculated using the following equations:

$$\mathbf{I} = \left(\frac{\mathbf{S}}{\mathbf{V_r}}\right)^*, \quad \mathbf{V_{s'_s}} = \mathbf{V_r} + \mathbf{IZ} - \mathbf{V_s} \tag{1}$$

where $\mathbf{S} = P_{ref} + jQ_{ref}$ and $\mathbf{Z} = R + jX$ the total impedance of the transmission line and the network. Once $|\mathbf{V_{s'_s}}|$ and β are determined, they are passed to the tap selection algorithm which then identifies the best tap positions for the compensating windings to approximate $|\mathbf{V_{s'_s}}|$ and β with minimum error.

4) Tap Selection Algorithm: The required series compensating voltage, $\mathbf{V_{s'_s}}$, in any phase is derived from the contributions of the compensating windings of the ST from three different phases. If the required phase angle, β of the series compensating voltage is exactly at 0°, 120° or 240°, it can be constructed from only one of the three phases a, c, or b, respectively. For any other angle, the series compensating voltage is constructed from two adjacent phases.

Consider the ST of Fig. 1, which has four tap positions in each of the nine compensating secondary windings. Each tap position provides a voltage of 0.05 p.u. and therefore, a maximum of 0.2 p.u. can be obtained from each phase. The possible combinations of voltage tap-setting positions are shown by the

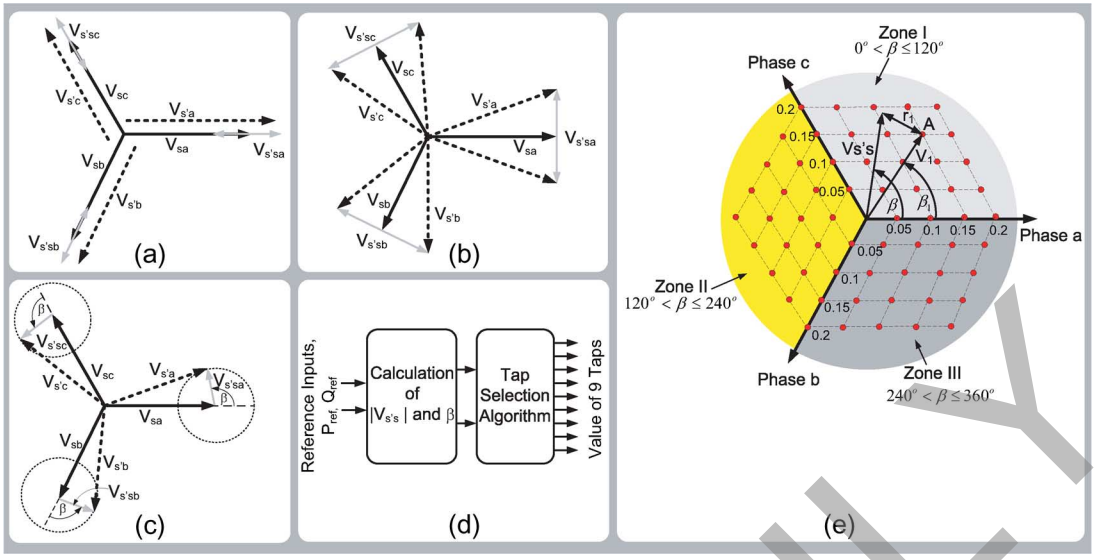

Fig. 2. Control modes of the ST. (a) Voltage regulator, (b) phase-angle regulator, (c) power-flow regulator, (d) control inputs and outputs, and (e) tap position grid for the construction of $\mathbf{V_{s's}}$ by selecting the best tap setting.

dotted grid in Fig. 2(e). Let $|\mathbf{V_{s's}}|$ be the required compensating voltage, at an angle $\boldsymbol{\beta}$ with reference to the corresponding phase angle. Then, one of the tap positions will be the nearest to the voltage phasor, $\mathbf{V_{s's}}$, which will yield the best approximation of $\mathbf{V_{s's}}$. The tap selection algorithm is designed to calculate the normalized vector distance of all the tap positions in the grid and then to identify the required tap position based on the minimum normalized vector distance. For example, in Fig. 2(e), the tap position A which is constructed by 0.15 p.u. injection from both phase a and phase c forms the vector V_1 at an angle, β_1 with respect to phase a. The vector $\mathbf{V_1}$ is away from $\mathbf{V_{s's}}$ by the normalized vector distance r_1, which is termed as the error ε_1 with respect to $\mathbf{V_{s's}}$ and given by

$$\varepsilon_1 = \|r_1\|_2 = \sqrt{(V_1^x - V_{s's}^x)^2 + (V_1^y - V_{s's}^y)^2} \tag{2}$$

where $V_{s's}^x$ and $V_{s's}^y$ denote the two rectangular components of $V_{s's}$ in the cartesian coordinate system. V_1^x and V_1^y are the corresponding Cartesian components of V_1. Similarly, the ε_k ($k = 1, 2, 3, 4$) with respect to $\mathbf{V_{s's}}$ will be determined for the four tap setting positions adjacent to $\mathbf{V_{s's}}$ (grid positions shown in Fig. 2(e)). The tap-setting combination corresponding to V_k with the smallest ε_k is selected as the best tap-setting to implement $\mathbf{V_{s's}}$. The detailed algorithm to determine the best tap-setting for $\mathbf{V_{s's}}$ is described in [3].

III. Detailed Transient Model of the ST

The ST is modeled as a twelve-winding transformer with three primary and nine secondary windings. Considering the schematic of the ST shown in Fig. 1, one can categorize the 12 different windings into four distinct sets of windings, as follows.

1) A, B, C (Primary windings (P)).
2) a_1, b_2, c_3. (First set of secondary windings (S1)).
3) a_2, b_3, c_1. (Second set of secondary windings (S2)).
4) a_3, b_1, c_2. (Third set of secondary windings (S3)).

The reason for grouping secondary windings in this manner is that the three secondary windings in each set undergo the same tap setting.

The modeling steps include:

1) development of linear equations for the ST and power system;
2) addition of nonlinear branches to the ST to model saturation;
3) inclusion of tap changing effect on the ST parameters.

A. Linear Model of the ST and Power System

The ST linear model is based on the BCTRAN model [4] of a transformer. The dynamic equation of the ST can be expressed as

$$\left[\frac{di}{dt}\right] = -[L_{ST}]^{-1}[R_{ST}][i] + [L_{ST}]^{-1}[v]. \tag{3}$$

In the above equation, $[i]$ and $[v]$ are the vectors of currents and voltages in the 12 windings of the ST, and $[R_{ST}]$ and $[L_{ST}]^{-1}$ are 12×12 matrices of the ST resistance and inverse inductance.

Despite the fact that the ST has twelve windings, due to the series connection between different secondary windings as shown in Fig. 1, there would only be six independent currents in the circuit; the three primary currents (i_{sa}, i_{sb}, and i_{sc}) and three secondary currents (i_a, i_b, and i_c) which are also the line currents. Therefore, the unknowns in (3) are six currents and nine voltages of the secondary windings. Considering the network and the ST as shown in Fig. 1, the voltages on the primary windings of the ST can be described in terms of unknown currents and voltage sources. Also, the following voltage equations can be derived:

$$\begin{aligned}
&L_s\frac{di_{sa}}{dt} + (L_s + L_{TL})\frac{di_a}{dt} + R_s i_{sa} + (R_s + R_{TL})i_a \\
&\quad = v_{a1} + v_{b1} + v_{c1} + v_a - v_{ra} \\
&L_s\frac{di_{sb}}{dt} + (L_s + L_{TL})\frac{di_b}{dt} + R_s i_{sb} + (R_s + R_{TL})i_b \\
&\quad = v_{a2} + v_{b2} + v_{c2} + v_b - v_{rb} \\
&L_s\frac{di_{sc}}{dt} + (L_s + L_{TL})\frac{di_c}{dt} + R_s i_{sc} + (R_s + R_{TL})i_c \\
&\quad = v_{a3} + v_{b3} + v_{c3} + v_c - v_{rc}
\end{aligned} \tag{4}$$

where v_{a1} to v_{c3} are the terminal voltages of the secondary windings a_1 to c_3. v_a, v_b, v_c, and v_{ra}, v_{rb}, v_{rc} are the sending-end and receiving-end voltage sources in each phase. L_s, L_{TL}, R_s, and R_{TL} are the source and transmission line inductance and resistance, respectively. Rearranging (3) and (4) in terms of unknown voltages and currents, the final system of equations for the ST and the power system can be expressed as the following matrix equation:

$$\mathbf{C}\dot{\mathbf{x}} = \mathbf{A}\mathbf{x} + \mathbf{B}\mathbf{u} \tag{5}$$

where

$$\mathbf{x} = [i_{sa} \quad i_{sb} \quad i_{sc} \quad i_a \quad i_b \quad i_c \quad v_{a1} \quad v_{b2} \quad v_{c3} \quad v_{a2} \quad v_{b3} \quad v_{c1} \quad v_{a3} \quad v_{b1} \quad v_{c2}]^T \tag{6}$$

and

$$\mathbf{u} = [v_a \quad v_b \quad v_c \quad v_{ra} \quad v_{rb} \quad v_{rc}]^T. \tag{7}$$

The $\mathbf{A}$, $\mathbf{B}$, and $\mathbf{C}$ matrices are calculated in terms of resistances and inductances of the electrical network and $[R_{ST}]$, $[L_{ST}]^{-1}$ matrices of the ST.

Since the voltage derivatives in (3) and (4) are all zeroes, matrix $\mathbf{C}$ is rank deficient and (5) would be a system of differential-algebraic equations (DAEs). Due to the strong coupling between different equations of the system, we preferred to keep (5) in its original format and solve all the equations together rather than separating the algebraic and differential equations from each other.

B. Saturation Effect

The nonlinear magnetizing inductance of the ST is modeled as a set of three two-slope piecewise linear inductances which are externally connected to the terminals of primary windings. The knee point of magnetizing curve is set to 1.5 times of rated flux, according to the data from the manufacturer. During the simulation, the flux linkages are estimated separately for each phase to decide the proper value of magnetizing inductances in each time-step. The equation for flux linkage estimation of the primary winding A is as follows:

$$\lambda_A = \int \left(V_{sa} - R_A i_{sa} - L_{\delta A} \frac{di_{sa}}{dt} \right) dt \tag{8}$$

where V_{sa} is the terminal voltage, and R_A and $L_{\delta A}$ are the resistance and leakage inductance of the primary winding A, respectively.

Fig. 3 shows the piece-wise linear approximation of the magnetizing curve of the ST. If the value of the estimated flux linkage in each phase is less than 1.5 p.u., the unsaturated magnetizing inductance (L_{m1}) will be connected to the primary terminal of that phase. Otherwise saturated magnetizing inductance (L_{m2}) will be used to model the saturation of the ST in the simulation.

C. Tap-Changing Effect on the ST Parameters

The inclusion of taps in the ST model is achieved by using appropriate base values to convert elements of $[L_{ST}]^{-1}$ from p.u. to real quantities, according to the following equation:

$$[L_{ST}]^{-1}_{ik} = [L^{p.u.}_{ST}]^{-1}_{ik} \frac{S_{rating}}{3V_i V_k} \tag{9}$$

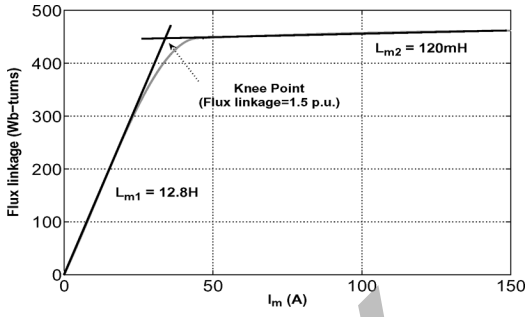

Fig. 3. Piece-wise linear approximation of the magnetizing curve of the ST.

where $[L_{ST}]^{-1}_{ik}$ represents the entry on the ith row and kth column of matrix $[L_{ST}]^{-1}$, S_{rating} is the three-phase power rating used as the common base for all p.u. values, V_i and V_k are the rated voltages of windings i and k in their corresponding tap positions.

Since the exact values of p.u. inductances for different tap positions were not available, it was assumed that the per-unit inductances of the ST were not affected by the tap position. Winding resistances of the ST are also determined for each tap position as follows:

$$[R_{ST}]'_j = \frac{V'_j}{V_j}[R_{ST}]_j \tag{10}$$

where $[R_{ST}]'_j$, $[R_{ST}]_j$, V_j, and V'_j are the resistance and rated voltage of jth winding at the current and full tap positions, respectively. Note that those elements of $[R_{ST}]$ and $[L_{ST}]^{-1}$ which are only related to the primary windings do not change during the simulation because there is no tap-changing mechanism on the primary windings. Since the magnetizing branches are connected to the primary side of the ST, the magnetizing inductances are also independent of tap position.

D. Time-Step Loop

In order to discretize (5), the Trapezoidal rule was used due to its well accepted accuracy and stability even with a comparatively large time-step. The time marching formula for the unknown vector $\mathbf{x}$ using this rule can be written as follows:

$$\mathbf{x}^{k+1} = \left(\mathbf{C} - \frac{\Delta t}{2}\mathbf{A} \right)^{-1} \times \left[\left(\mathbf{C} + \frac{\Delta t}{2}\mathbf{A} \right) \mathbf{x}^k + \frac{\Delta t}{2}\mathbf{B}(\mathbf{u}^k + \mathbf{u}^{k+1}) \right] \tag{11}$$

where the superscripts $(k+1)$ and (k) denote the values of different quantities in the present and previous time-steps, respectively.

Switching events occur in the system due to the tap changing as well as saturation of the ST core. Also the numerical solutions of differential-algebraic equations (DAEs) are well known for their tendency to drift away from the manifold which is defined by a set of algebraic equations that must be satisfied by system state variables at each time-step [6]. A common method to suppress unrealistic oscillations in the simulation results as well as avoiding the drift error is to use a combination of Backward Euler method and trapezoidal rule which is referred to as the critical damping adjustment (CDA) [7]. Therefore, we begin the simulation with trapezoidal rule until reaching a switching

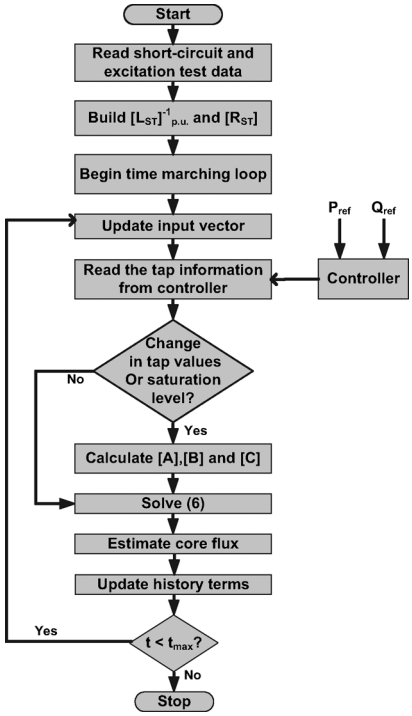

Fig. 4. Flowchart of the ST transient simulation.

point or convergence problem, then switched to the backward Euler method for a few steps followed by trapezoidal steps. The time-step of backward Euler is set to be half of that of the trapezoidal method in order to use the same $\mathbf{A}$, $\mathbf{B}$, and $\mathbf{C}$ matrices for both methods.

The complete simulation of the ST requires the simulation of two parts: 1) the electrical system which consists of the ST and the power system models and 2) the control system. In the electrical system model, per-unit elements of $[L_{ST}]^{-1}$ are calculated once at the very beginning of the program from short circuit and excitation test data at the full tap position of all secondary windings. These values are given in Table III.

With these p.u. values, the time marching loop begins after receiving the tap position information from the controller in order to regulate the active and reactive powers to the desired level. If there is any change in the tap positions, per-unit inductances are converted to real values according to the new tap information and winding resistances are also updated. In the case of entering or leaving the saturation state, the values of magnetizing inductances are adjusted accordingly. The $\mathbf{A}$, $\mathbf{B}$, and $\mathbf{C}$ matrices are then calculated from the new values of $[L_{ST}]^{-1}$ and $[R_{ST}]$. Finally, (11) is solved to obtain the unknown vector of $\mathbf{x}$ for the current time-step. The time marching loop continues until another change in power level is requested by the controller or saturation state of the ST changes. The flow chart of the simulation program is given in Fig. 4.

IV. Real-Time Implementation

The real-time simulation of the ST and its controller was carried out on a state-of-the-art PC-Cluster based real-time simulator [8].

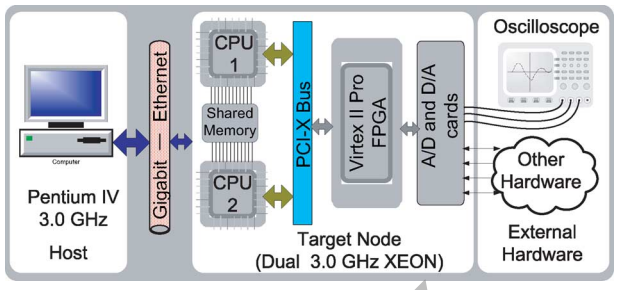

Fig. 5. Architecture of the simulator for the real-time simulation of the ST.

A. Simulator Details

The simulator is built out of a high-speed computer known as the target which works as the main computational engine, and the host which is used for model development and monitoring the results. FPGA based I/Os provide external communication, and a gigabit ethernet network is used for communication between the computers. The target processors are 3.0 GHz dual Intel Xeon and the host processor is 3.0 GHz Pentium IV. Fig. 5 shows the simulator setup. The target computer runs on a Linux based real-time operating system which offers eXtra High Performance (XHP) mode operation through CPU shielding where one CPU is dedicated for the simulation while the other CPU is responsible for running the OS and other jobs such as interrupt handling, writing to the disk and I/O operations. The host computer runs on Windows XP on which a real-time interfacing software RT-LAB [9] from Opal RT Technologies, Inc., is installed to perform the co-ordination of all the hardware involved in the simulation. MATLAB/SIMULINK and SimPowerSystem toolbox along with other toolboxes are used to prepare the model for simulation. Real-time simulation results are observed through an oscilloscope connected to the I/O terminals of the target node.

B. Real-Time Implementation of the ST Model and Controller

As mentioned earlier, there is no readily available model for the ST in a commercial transient simulation program, therefore, the entire system was coded using C language and embedded as a dynamically linked program (S-function) in the SIMULINK model. SIMULINK uses state-space approach to solve the system, on the other hand, EMTP model of the ST is based on DAEs. To perform a transient simulation of the ST in the MATLAB/SIMULINK environment, S-function is, therefore, the best option.

V. Results and Analysis

All the off-line and real-time simulations are performed using a time step of 100 μs. In these simulations, it is assumed that each secondary winding is capable of injecting up to 0.4 p.u. series voltage in the line (9 tap positions for each secondary winding), although in Fig. 1 only 5 tap positions are shown. Before injecting any series voltage, the system was simulated in an uncompensated mode with the network parameters listed

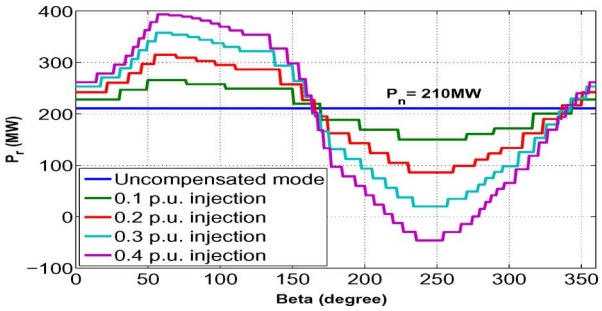

Fig. 6. Active power P_r for various magnitudes of injected voltage at varying angle β.

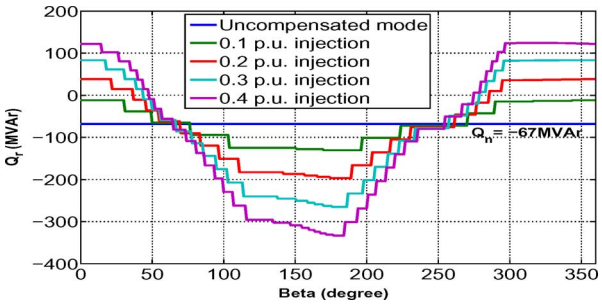

Fig. 7. Reactive power Q_r for various magnitudes of injected voltage at varying angle β.

in Table III. The equations used for the calculation of instantaneous active and reactive power at the receiving end, are as follows:

$$P_r = (v_a i_a + v_b i_b + v_c i_c), \quad Q_r = \sqrt{3}(v_a i_c - v_c i_a). \quad (12)$$

In an uncompensated mode, P_r and Q_r become natural power flows and are denoted by P_n and Q_n. In the compensated mode, with the ST rating of 30 MVA, the following cases have been simulated.

- Case I: Steady-state performance of the ST when β is varied between 0° and 360° while $|\mathbf{V_{s's}}|$ is kept constant between 0.1 to 0.4 p.u. with a step of 0.1 p.u.
- Case II: Transient response of the ST showing the energization and the step responses of active and reactive power demand.

A. Case I: Steady-State Results

In this case, the simulation of the ST is carried out for a compensated series voltage of 0.1 p.u. to 0.4 p.u. The angle β is varied at a discrete step of 1° in the range of 0° to 360° for a tap resolution of 5%. The variation of both P_r and Q_r are shown in Fig. 6 and Fig. 7, respectively, for four magnitudes of injected voltage as well as the uncompensated mode (zero voltage injection).

It is evident that both of the active and reactive power follow an almost first-order-hold sinusoidal pattern by varying the phase angle. Nevertheless, looking at the active power profile, it can be seen that the difference between the peak magnitude of the compensated and uncompensated active power in the first half cycle is smaller than that in the second half cycle. In other words, the ST has a higher capacity when regulating

TABLE I
TAP POSITIONS OF THE ST SECONDARY WINDINGS FOR FOUR EXTREME CASES

	Tap Position		
Power Level	**S1**	**S2**	**S3**
$P_r^{\max}$	Full	Full	0
$P_r^{\min}$	0	0	Full
$Q_r^{\max}$	Full	0	0
$Q_r^{\min}$	0	Full	Full

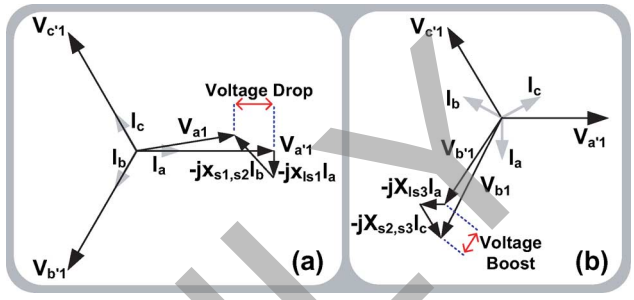

Fig. 8. (a) Phasor diagram of V_{a1} during the high levels of positive active power (P_r) and (b) phasor diagram of V_{b1} during the high levels of negative reactive power (Q_r).

active power below the natural power rather than above it. The reason for this asymmetry in the behavior of the ST can be described as follows. As we reach the peak magnitude of active power, a large amount of in-phase currents flow through the transmission line and ST impedances, which results in a large voltage drop across these impedances. Also, the ST is modeled as a set of 12 coupled windings with nonzero coupling coefficients between the secondary windings. This means that if more than one secondary winding has a non-zero tap value, then there would be a secondary effect voltage drop or voltage boost in the ST injected voltage due to the currents flowing through the other secondary windings.

Table I shows the tap positions of the ST secondary windings for four extreme values of P_r and Q_r. As can be seen, at the peak magnitude of active power $(P_r^{\max})$ secondary windings of S1 and S2 are in series with the line and both of them are in their full tap positions (maximum resistance and inductance). The effect of interaction of these two sets of secondary winding on the ST injected voltage at high levels of active power can be explained by the phasor diagram shown in Fig. 8(a), which is drawn based on the following assumptions.

- Resistances of secondary windings are neglected.
- All the inter-phase coupling coefficients are assumed to be zero; in practice inter-phase couplings are very small compared to same-phase couplings.
- Quadrature component of line current is neglected in the peak value of active power; in the simulation results it was about 7% of the in-phase component.

The phasor equation for $\mathbf{V_{a1}}$ which is the output voltage of a_1, one of the S1 windings in series with phase A, can be described as follows:

$$\mathbf{V_{a1}} = \mathbf{V_{a'1}} - jX_{ls1}\mathbf{I_a} - jX_{s1,s2}\mathbf{I_b}. \quad (13)$$

$\mathbf{V_{a'1}}$ denotes the induced voltage in a_1 from the primary side. Neglecting the small voltage drop due to the sending-end source and the ST primary winding impedances, this voltage is almost

equal to the rated voltage of the secondary windings (0.4 p.u.), and is in phase with phase A of the sending-end voltage. The phasor voltage due to the leakage inductance of $a_1(-jX_{ls1}\mathbf{I_a})$ is added to $\mathbf{V_{a'1}}$. Also because of the phase B current flowing through the other coil coupled to phase A (a_2), an extra phasor $(-jX_{s1,s2}\mathbf{I_b})$ denoting the effect of mutual inductance between a_1 and a_2 is added to $\mathbf{V_{a'1}}$. Note that the value of mutual inductance between a_1 and a_2 is larger than the leakage inductance of a_1. The net effect of adding these two phasors would result in a considerable voltage drop, and a small phase shift across the terminals of a_1, as shown in Fig. 8(a). At the highest level of active power the value of this voltage drop reaches about 11% of rated voltage. Almost the same voltage drop would appear on the terminals of c_1 which will further decrease the value of active power on the line. This effect does not appear in the negative peak of active power (P_r^{min}) since the current flowing through the line is small, and there is only one set of secondary windings (S3) in series with the line. The amount of asymmetry between the two half cycles become smaller as the magnitude of the desired injected voltage decreases, which can be seen from Fig. 6.

For the case of reactive power, the situation is reversed; flow of high quadrature current in the line will increase the ST injected voltage rather than decreasing it. This can be seen from Fig. 7, where the distance between the negative peak value of Q_r and Q_n is larger than the distance between positive peak value of Q_r and Q_n.

This effect can be described by the use of a phasor diagram shown in Fig. 8(b). In this case the line current is assumed to be in quadrature with the sending-end voltage. Now consider the peak magnitude of Q_r in the negative direction $(Q_r^{\min})$, when from Table I the secondary windings of S2 and S3 are at their full tap positions. The phasor equation for $\mathbf{V_{b1}}$ which is the output voltage of b_1, one of the S3 windings in series with phase A, can be written as

$$\mathbf{V_{b1}} = \mathbf{V_{b'1}} - jX_{ls3}\mathbf{I_a} - jX_{s2,s3}\mathbf{I_c}. \tag{14}$$

Again, two phasors are added to the induced voltage by the primary side in b_1—one due to the phase A current flowing through the leakage inductance of $b_1(-jX_{ls3}\mathbf{I_a})$, and the other due to the phase C current flowing through the other winding coupled to phase B (b_3), which is equal to $-jX_{s2,s3}\mathbf{I_c}$. The net effect is a small voltage boost and phase shift in the series injected voltage and thus a higher negative peak for Q_r.

It is to be noted that if separate units (zero mutual couplings) are used for different sets of secondary windings, the mutual effect of secondaries on each other will be eliminated and the above asymmetry in active and reactive powers will disappear.

The relationship between P_r and Q_r for $V_{s's}$ of 0.1 p.u., 0.2 p.u., 0.3 p.u., and 0.4 p.u. is shown in Fig. 9. It was found that the ST produces a nearly hexagon profile compared to the circular profile of UPFC [2].

B. Case II: Transient Results

Real-time transient simulation of the model begins with the energization of the ST and power system in the uncompensated mode. As expected, inrush currents flow through the primary winding of the ST at the beginning. The magnitude of inrush current in each phase depends on the instant of energizing the system. Fig. 10 shows the real-time inrush currents for a number

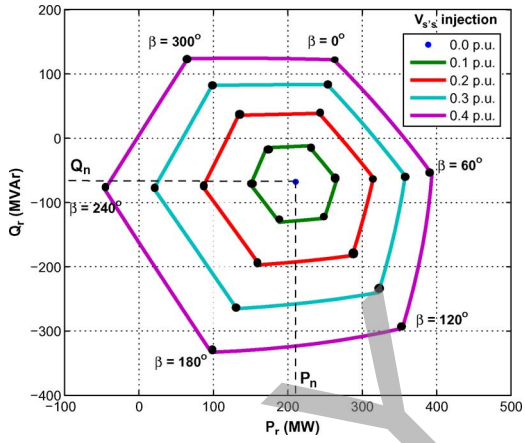

Fig. 9. Relationship between P_r and Q_r at various phase angle, β and series voltage, $V_{s's}$ for the ST.

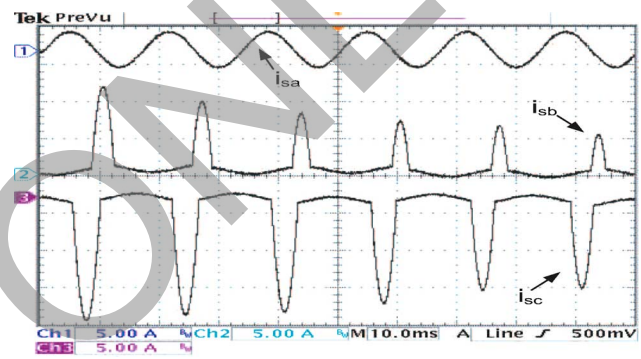

Fig. 10. Real-time oscilloscope trace of inrush currents i_{sa} A (×0.1), i_{sb} A (×0.02) and i_{sc} A (×0.02) in the primary windings of the ST when the system is energized at $\omega t = \pi/2$ (Ch1 Max = 2.8 A, Ch2 Max = 11.8 A, Ch3 Min = −16.6 A).

of cycles, when the system is energized at $\omega t = \pi/2$. It can be seen that the current flowing through phase A (i_{sa}) is in the sinusoidal steady-state mode from the beginning while phases B and C carry a relatively large magnitude of inrush currents (i_{sb} and i_{sc}) which decay slowly to the steady-state. The peak magnitude of the inrush current at no-load condition happens in phase C and reach 140% of the ST rated current. In the uncompensated mode the natural powers P_n and Q_n are equal to 210 MW and −67 MVAr, respectively, shown by a small dot at the center of Fig. 9 when $\mathbf{V_{s's}} = 0$ p.u..

Fig. 11 shows the real-time transient response of P_r and Q_r over 40 s of simulation time. At $t_1 = 5$ s an injected voltage of 0.25 p.u. magnitude with the phase angle of 0° is requested by the controller, which means that the secondary windings of S1 should be placed at the tap position of 0.25 p.u. In this simulation a 5% tap-to-tap voltage is assumed, so that reaching the tap position of 0.25 p.u. for one set of windings will take 5 steps. Each step of the tap changing transition will take 2 s thus requiring 10 s to complete the transition at $t_2 = 15$ s. During this period of transition the reactive power Q_r begins to increase and becomes positive (65 MVAr) at t_2. There would also be some increase (40 MW) in the value of P_r, but since the injected voltages are in phase with the line voltages the amount of change in Q_r is larger than that of P_r.

At $t_3 = 19.2$ s active power reversal is requested by the controller. In this case secondary windings of S1 and S2 will be

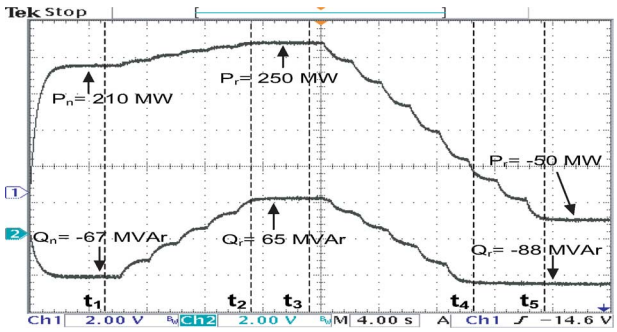

Fig. 11. Real-time oscilloscope trace of transient response of P_r MW ($\times 1/30$) and Q_r MVAr ($\times 1/30$) for injected voltage demand of 0.25 $\angle$ 0 p.u. at t_1 and active power reversal demand at t_3.

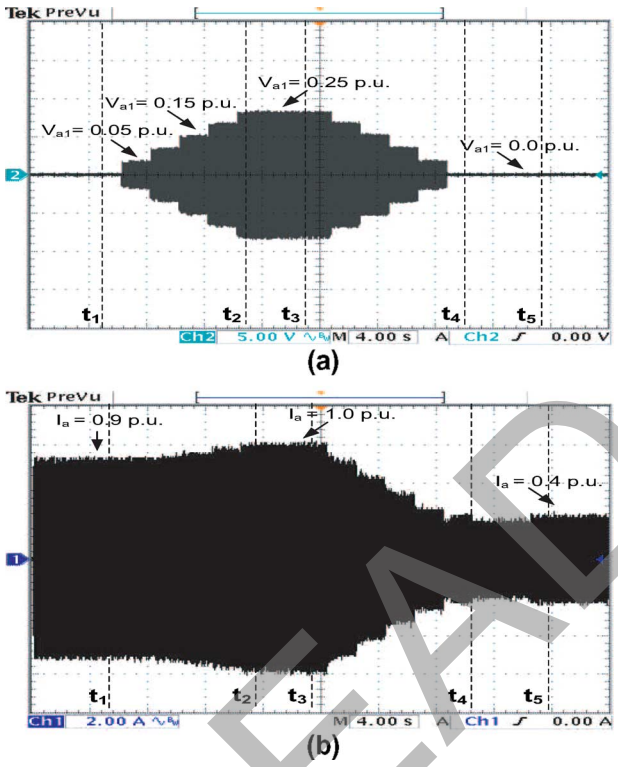

Fig. 12. Real-time oscilloscope trace of transient response of (a) v_{a1} kV ($\times 1/3$) and (b) i_a kA ($\times 4$) for injected voltage demand of 0.25 $\angle$ 0 p.u. at t_1 and active power reversal demand at t_3 (Ch1 pk $-$ pk $= 12.3$ A, Ch2 pk $-$ pk $=$ 17 V).

placed at zero tap positions and S3 windings will reach their full tap position (0.4 p.u.) through 8 steps. The step by step decrease in the value of P_r from 250 MW at $t_3 = 19.2$ s to -50 MW at $t_5 = 35.2$ s can be seen in Fig. 11. During this period Q_r will also decrease until reaching the steady-state value of -88 MVAr at $t_4 = 30$ s. In the final steps of tap transition (from t_4 to t_5) the value of Q_r does not change since the angle of injected voltage is constant (240°) and only its magnitude is increasing from 0.2 p.u. to 0.4 p.u.

Fig. 12 shows the transient behavior of injected voltage by winding $a_1(v_{a1})$ and line current in phase A (i_a) over the same 40 s interval as that of Fig. 11. The step by step change in the value of injected voltage by changing the tap position from 0 to 0.25 p.u. and then coming back to the zero tap position can

TABLE II
EXECUTION TIME FOR INDIVIDUAL TASKS WITHIN ONE TIME-STEP

Task	Execution Time (μs)
Computation Time	75.452670
Idle Time	22.445000
Data Acquisition	1.247333
Status Update	0.187333
Target Request Handling	0.042333
Host Request Handling	0.323330
Synchronization Handling	0.040000
Others	0.262001
Total Step-Size	100.000000

TABLE III
DATA FOR THE ELECTRICAL SYSTEM AND THE ST

Power System Parameters	Value
Base values	240MVA and 138kV
Sending end and receiving end voltage	$1\angle 0°$ p.u. and $1\angle -20°$ p.u.
Source impedance at the sending-end	1.0053Ω and 19.17mH
Transmission line impedance	3.0159Ω and 59.19mH
Rating of the ST transformer	30MVA
ST Short-Circuit Impedances	**Value**
$Z_{P,S1}, Z_{P,S2}, Z_{P,S3}$ (positive sequence)	17.77Ω
$Z_{P,S1}, Z_{P,S2}, Z_{P,S3}$ (zero sequence)	17.17Ω
$Z_{S1,S2}, Z_{S1,S3}, Z_{S2,S3}$ (positive sequence)	7.12Ω
$Z_{S1,S2}, Z_{S1,S3}, Z_{S2,S3}$ (zero sequence)	6.9Ω
ST Resistances	**Value**
Primary winding resistance (per phase)	0.893Ω
S1, S2, S3 winding resistance (per phase)	0.298Ω
Magnetizing Characteristic of ST	**Value**
Saturation curve knee point	1.5 times rated flux
Unsaturated magnetizing inductance	12.8H
Saturated magnetizing inductance	120mH

be clearly seen in this figure. The magnitude of line current is also decreasing during the active power reversal period since the absolute value of active power in the negative direction (50 MW) is much smaller than the natural active power of the system (210 MW).

C. Execution Time

A detailed breakdown of the execution time for a single time-step of the real-time simulation is shown in Table II. As expected, computation time is the most time-consuming task within each time-step due to the large number of vector and matrix operations in the program. Although running the real-time simulation with even a smaller time-step is achievable, an idle time of about 22 μs is preserved to avoid any overruns during dynamic changes of input/output parameters and have the flexibility to increase the number of hardware I/Os.

XHP mode was also enabled during the real-time simulation because it was found that sharing the computational task between the two processors of a target node would result in an excessive communication time and prevent the simulation with a time-step of 100 μs to run in real-time.

VI. CONCLUSION

The ST is a unique device for controlling voltage, phase-angle and power flow in a transmission network. Despite its relatively slower response in comparison to the UPFC, the advantages of the ST lie in the simplicity of its control, the absence of unnecessary complexity of power electronics, and the overall lower cost and higher-efficiency of the power-flow controller. Up to now

a detailed transient model of the ST was not available, which prompted users to employ approximate models of simplified transformers available in EMTP-type programs. This precluded transparency in the simulation and control design stages. This paper has developed an accurate ST transient model from realistic components thus providing greater insight into the ST functionality. The two salient features of this model are the effect of mutual coupling in the ST secondary windings, and the nonlinear excitation characteristic heretofore ignored in the previous works. The inclusion of these effects made the ST model developed more realistic. This also opens the way for incorporating the model into commercial EMTP-type programs.

Real-time implementation of the entire system model and the controller was carried out on a state-of-the-art simulator. The real-time simulation is fully interactive as though the user is communicating with the real system. Real-time oscilloscope results are given to demonstrate the performance of the model and the controller. The execution time of the simulation is quite low; on a 100 μs time-step the ST model execution is only 75 μs. These numbers show that the developed ST model is computationally efficient, and that the control algorithm is suitable for online applications.

REFERENCES

[1] K. K. Sen and M. L. Sen, "Introducing the family of "sen" transformers: A set of power flow controlling transformers," *IEEE Trans. Power Del.*, vol. 18, no. 1, pp. 149–157, Jan. 2003.

[2] K. K. Sen and M. L. Sen, "Comparison of the "sen" transformer with the unified power flow controller," *IEEE Trans. Power Del.*, vol. 18, no. 4, pp. 1523–1533, Oct. 2003.

[3] M. O. Faruque and V. Dinavahi, "A tap-changing algorithm for the implementation of "sen" transformer," *IEEE Trans. Power Del.*, vol. 22, no. 3, pp. 1750–1757, Jul. 2007.

[4] V. Brandwajn, H. W. Dommel, and I. I. Dommel, "Matrix representation of three-phase n-winding transformers for steady-state and transient studies," *IEEE Trans. Power App. Syst.*, vol. PAS-101, no. 6, pp. 1369–1378, Jun. 1982.

[5] Reinhausen Manuf., Load Tap Changer, Type RMV-A Instruction manual, TL 8001.01, pp. 5–12.

[6] K. E. Brenan, S. L. Campbell, and L. R. Petzold, *Numerical Solution of Initial-Value Problems in Differential-Algebraic Equations*. New York: Elsevier, 1989.

[7] J. R. Marti and J. Lin, "Suppression of numerical oscillations in the EMTP," *IEEE Trans. Power Syst.*, vol. 4, no. 2, pp. 739–747, May 1989.

[8] L.-F. Pak, M. O. Faruque, X. Nie, and V. Dinavahi, "A versatile cluster-based real-time digital simulator for power engineering research," *IEEE Trans. Power Syst.*, vol. 21, no. 2, pp. 455–465, May 2006.

[9] *"RT-LAB 8.x Users Manual,"* Opal-RT Technology Inc., Montreal, QC, Canada, 2006, pp. 1–80.

Babak Asghari (S'06) received the B.Sc. and M.Sc. degrees in electrical engineering from Sharif University of Technology, Tehran, Iran, and is currently pursuing the Ph.D. degree in the electrical and computer engineering at the University of Alberta, Edmonton, AB, Canada.

His research interests include real-time digital simulation and control of power systems and electrical drives.

M. Omar Faruque (S'03) received the B.Sc. .Eng. degree from Chittagong University of Engineering and Technology (CUET), Bangladesh, in 1992, and the M.Eng.Sc. degree from the University of Malaya, Malaysia, in 1999, and is currently pursuing the Ph.D. degree in electrical and computer engineering at the University of Alberta, Edmonton, AB, Canada.

He worked in both industry and academia prior to starting his Ph.D. program. His research interests include FACTS, HVDC, and real-time digital simulation and control of power electronics and power systems.

Venkata Dinavahi (M'00) received the Ph.D. degree from the University of Toronto, Toronto, ON, Canada, in 2000.

He is an Associate Professor at the University of Alberta, Edmonton, AB, Canada. His main research interests are in the areas of real-time simulation, electromagnetic transients, power electronics, and digital control.